ACS OMEGA

Open Access

http://pubs.acs.org/journal/acsodf

Article

Effect of Main and Side Chains on the Folding Mechanism of the Trp-Cage Miniprotein

Yutaka Maruyama* and Ayori Mitsutake

Cite This: *ACS Omega* 2023, 8, 43827−43835

Read Online

ACCESS | Metrics & More | Article Recommendations

ABSTRACT: Proteins that do not fold into their functional native state have been linked to diseases. In this study, the influence of the main and side chains of individual amino acids on the folding of the tryptophan cage (Trp-cage), a designed 20-residue miniprotein, was analyzed. For this purpose, we calculated the solvation free energy (SFE) contributions of individual atoms by using the 3D-reference interaction site model with the atomic decomposition method. The mechanism by which the Trp-cage is stabilized during the folding process was examined by calculating the total energy, which is the sum of the conformational energy and SFE. The folding process of the Trp-cage resulted in a stable native state, with a total energy that was 62.4 kcal/mol lower than that of the unfolded state. The solvation entropy, which is considered to be responsible for the hydrophobic effect, contributed 31.3 kcal/mol to structural stabilization. In other words, the contribution of the solvation entropy accounted for approximately half of the total contribution to Trp-cage folding. The hydrophobic core centered on Trp6 contributed 15.6 kcal/mol to the total energy, whereas the solvation entropy contribution was 6.3 kcal/mol. The salt bridge formed by the hydrophilic side chains of Asp9 and Arg16 contributed 10.9 and 5.0 kcal/mol, respectively. This indicates that not only the hydrophobic core but also the salt bridge of the hydrophilic side chains gain solvation entropy and contribute to stabilizing the native structure of the Trp-cage.

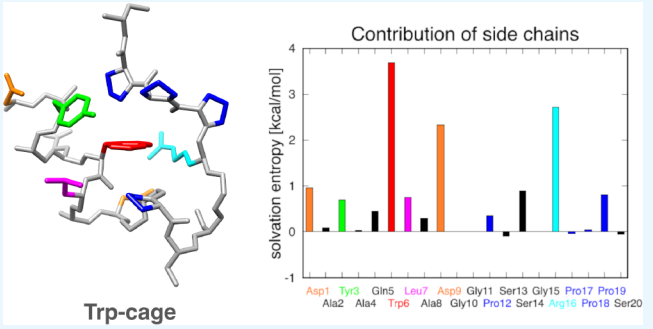

INTRODUCTION

Understanding protein folding is of fundamental importance in molecular biology. The advent of neural-network-based structure prediction programs such as AlphaFold2[1] and RoseTTAFold[2] enables native structures to be predicted with high accuracy using amino acid sequences. This is expected to greatly accelerate research on protein structures. However, the ability to predict the native structure does not mean that the protein folding mechanism is fully understood. For example, protein folding and misfolding are associated with several diseases. The fact that knowledge of the native structure is insufficient to identify and treat these diseases has motivated many theorists and experimentalists to study the protein-folding problem. We are particularly interested in the interaction between proteins and the surrounding water, which we study numerically.[3−7]

The 20-residue tryptophan-cage (Trp-cage) miniprotein, designed by Neidigh et al. and consisting of a Trp residue confined by a hydrophobic core, is a useful compact model protein that is often used to study protein-folding and stability.[8] Understanding the contribution of the hydrophobic core to the overall stability of the Trp-cage is of significant interest in protein-folding studies and has implications in protein engineering.[9−22] This protein is known to fold spontaneously and cooperatively in ∼4 μs,[10] whereas a variant thereof folds in ∼1 μs at room temperature.[23] The Trp-cage is therefore highly appropriate for studying the folding processes of peptides, both experimentally[11,24,25] and theoretically,[22,26−36] and in combination.[37,38] The Trp-cage has also been used as a test system for various new methods.[13,39−55] Many studies have shown that the Trp-cage can also exist in the form of metastable non-native states, which makes it useful for studying complex folding processes.[14,42,43,50,53−59]

Figure 1 shows the native structure of the Trp-cage variant (DAYAQWLADGGPSSGRPPPS), with a focus on certain side chains. The Leu, Trp, and Pro residues are hydrophobic, whereas Tyr and Arg are hydrophilic. The Trp-cage consists of a short α-helix from residues 2 to 8, a 3_{10}-helix from residues 11 to 14, and a C-terminal polyproline II helix packed against the central tryptophan side chain. The side chain of Trp6 is in contact with the side chain of Tyr3,[10,12,20,38,60] Leu7, Pro12,[16,40] Arg16,[58] Pro18, and Pro19,[10,11,61] but not in

Received: August 7, 2023
Revised: September 19, 2023
Accepted: October 27, 2023
Published: November 9, 2023

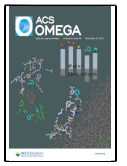

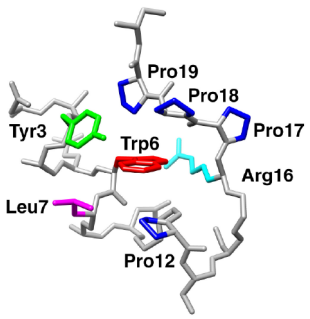

Figure 1. Backbone structures with selected side chains. In the native structure, the side chain of Trp6 is in contact with the side chains of Tyr3, Leu7, Pro12, Arg16, Pro18, and Pro19. The side chain of Pro17 is exposed to the solvent without contact with the side chain of Trp6.

contact with the side chain of Pro17. These side chains form the hydrophobic core of the Trp-cage, which plays a crucial role in maintaining its structural stability.[9−2260] The rotamer of the Trp6 side chain is the rate-limiting factor that governs the folding rate.[21,62,63] In addition to the hydrophobic core, the formation of a salt bridge between Asp9 and Arg16 also contributes to the structural stability of the Trp-cage.[10−12,14,16,27,53,57,61,64−68] The interaction responsible for the formation of the hydrophobic core is driven by the solvation entropy, which indicates a many-body interaction with the surrounding solvent. During the folding process, the side chains that form the salt bridge are dehydrated. Hence, the interactions with the surrounding solvent should be considered during the protein-folding process.[69]

The three-dimensional reference interaction site model (3D-RISM) theory is useful for investigating the interaction of a protein with its surrounding solvents. By combining this theory with the atomic decomposition method developed by Chang and Ham,[70−72] we calculated the solvation free energy (SFE) and solvation entropy at individual amino acid residues. Previously, we investigated the protein-folding mechanism of chignolin, a 10-amino acid miniprotein, by studying the influence of the main and side chains on the stability of protein. The native and misfolded states were found to have similar total energies but with a different composition, with side-chain interactions and hydrogen bonding playing crucial roles. Thus, we predicted that the mutation of Thr8 to a neutral amino acid could stabilize the misfolded structure over the native structure.[5] We calculated the stability of various structures in which the eighth residue was mutated and found that the T8P mutant stabilizes in the misfolded structure. In addition, NMR analysis of the T8P mutant supported these results.[6]

In this paper, we present a comprehensive analysis of the SFE and the solvation entropy contributions of amino acids in the hydrophobic core and salt bridge of the Trp cage using the atomic decomposition method. Our study aimed to elucidate the specific amino acids and their side chains that contribute significantly to the stability of the Trp-cage. By quantifying the solvation free energy and solvation entropy of each residue, we identified the key residues involved in stabilizing interactions and gained insights into the driving forces behind the structural stability of the Trp-cage.

METHOD

We introduce total energy G, which is the sum of the conformational energy E and SFE $\Delta\mu$:

$$G = E + \Delta\mu \tag{1}$$

As shown in previous studies, the conformational energy and the SFE are in competition with each other.[3−5,73] The $\Delta\mu$ term consists of two components: the solvation energy, E_s, and the solvation entropy, ΔS:

$$\Delta\mu = E_s - T\Delta S \tag{2}$$

where T denotes the temperature. Hereafter, $-T\Delta S$ with an energy dimension is termed the solvation entropy term. Evaluating the total energy provides a useful measure of protein structural stability.[3−75573] These components can be decomposed into the contributions of individual amino acids i, as follows:

$$E = \sum_{i}^{n} E_i \tag{3}$$

and

$$\Delta\mu = \sum_{i}^{n} \Delta\mu_i \tag{4}$$

where n represents the number of amino acids in the protein. These individual contributions are further divided into contributions from the main and side chains,

$$E_i = E_i^{\mathrm{M}} + E_i^{\mathrm{S}} \tag{5}$$

and

$$\Delta\mu_i = \Delta\mu_i^{\mathrm{M}} + \Delta\mu_i^{\mathrm{S}} \tag{6}$$

where M and S represent the main chain and side chains, respectively. The solvation energy and entropy terms are similarly divisible.

The conformational energy of a protein is determined by its structure and is influenced by various energy terms, including van der Waals, electrostatic, bond stretching, angle bending, and torsional energies. The van der Waals, electrostatic, and bond stretching energy terms are two-body potentials that are evenly divided among interacting atoms. However, the division of the energy terms for the angle bending and torsional potentials is not well-defined. Nevertheless, their effects are relatively small, because they exhibit low standard deviation. Therefore, for three- or four-body potentials, the energy term is considered to be equally distributed among the interacting atoms. Molecular mechanics and molecular dynamics programs are commonly used to calculate the energy terms.

The SFE represents the change in chemical energy when a solute molecule is transferred from one position in the gas phase to another in the solvent. Several methods can be employed to calculate the SFE, including the 3D-RISM theory.[74,75]

In this study, we considered the SFE of not only the whole protein but also of individual atoms using the atomic decomposition method.[70,72] This method calculates the SFE by considering the solute−solvent interaction and the solvent distribution function around the solute. The interaction potential acting on solvent site γ at position $\mathbf{r}$ is denoted by $u_\gamma(\mathbf{r})$. The distribution function of the solvent site, γ, around the solute is expressed by $g_\gamma(\mathbf{r})(=h_\gamma(\mathbf{r}) + 1)$, where $h_\gamma(\mathbf{r})$ is the total correlation function. The SFE is given by the Kirkwood charging formula:[76]

https://doi.org/10.1021/acsomega.3c05809
ACS Omega 2023, 8, 43827−43835

$$\Delta\mu = \sum_{\gamma} \rho_{\gamma} \int_0^1 d\lambda \int d\mathbf{r} \frac{\partial u_{\gamma}(\mathbf{r};\lambda)}{\partial\lambda} g_{\gamma}(\mathbf{r};\lambda) \tag{7}$$

where ρ_γ denotes the average number density of solvent site γ. The coupling parameter, λ, was used to gradually modify the interaction potential from $\lambda = 0$ (no interaction) to 1 (full interaction). $u(\mathbf{r};\lambda)$ varies with λ, and the distribution function under $u(\mathbf{r};\lambda)$ is denoted by $g(\mathbf{r};\lambda)$. $\Delta\mu$ represents the SFE of the whole solute, and we aimed to decompose it into the contributions from the individual atoms. $u_\gamma(\mathbf{r};\lambda)$ is expressed as a sum of the potentials between the atomic site of the solute, α, and the solvent site, γ, as follows:

$$u_{\gamma}(\mathbf{r};\lambda) = \sum_{\alpha=1}^{N} u_{\alpha\gamma}(|\mathbf{r} - \mathbf{r}_{\alpha}|;\lambda) \tag{8}$$

where $\mathbf{r}_\alpha$ is the position of the atomic site α and N is the number of atomic sites in the solute. Thus, the following basic expressions are obtained from eqs 7 and 8:

$$\Delta\mu = \sum_{\alpha=1}^{N} \Delta\mu_{\alpha} \tag{9}$$

and

$$\Delta\mu_{\alpha} = \sum_{\gamma} \rho_{\gamma} \int_0^1 d\lambda \int d\mathbf{r} \frac{\partial u_{\alpha\gamma}(|\mathbf{r} - \mathbf{r}_{\alpha}|;\lambda)}{\partial\lambda} g_{\gamma}(\mathbf{r};\lambda) \tag{10}$$

Notably, $u_{\alpha\gamma}(r;\lambda)$ has been decomposed into the potentials between atom α in the protein and solvent, while $g(r;\lambda)$ remains the distribution function with respect to the whole protein. The solute−solvent interaction potential, $u_{\alpha\gamma}(r)$, can be expressed as a combination of Lennard−Jones (LJ) and electrostatic potentials. The SFE contribution, $\Delta\mu_\alpha$, can be calculated by using the charging formula with two coupling parameters, λ_1 and λ_2. Thus, the solute−solvent interaction potential becomes

$$u_{\alpha\gamma}(r;\lambda_1,\lambda_2) = u_{\alpha\gamma}^{\mathrm{LJ}}(r;\lambda_1) + u_{\alpha\gamma}^{\mathrm{elec}}(r;\lambda_2) \tag{11}$$

Here,

$$u_{\alpha\gamma}^{\mathrm{LJ}}(r;\lambda_1) = 4\epsilon_{\alpha\gamma}\left[\left(\frac{\sigma_{\alpha\gamma}\lambda_1}{r}\right)^{12} - \left(\frac{\sigma_{\alpha\gamma}\lambda_1}{r}\right)^{6}\right] \tag{12}$$

and

$$u_{\alpha\gamma}^{\mathrm{elec}}(r;\lambda_2) = \frac{q_{\alpha}q_{\gamma}\lambda_2}{r} \tag{13}$$

where $\epsilon_{\alpha\gamma}$ and $\sigma_{\alpha\gamma}$ are the LJ parameters and q_α and q_γ are atomic charges. Thus, the integration path for λ_1 and λ_2 is as follows. First, the LJ interaction is performed from 0 to 1 with $\lambda_2 = 0$, after which the electrostatic interaction is switched on by integrating λ_2 from 0 to 1 while keeping $\lambda_1 = 1$. Finally, $\Delta\mu_\alpha$ is expressed as

$$\begin{aligned}\Delta\mu_{\alpha} = \sum_{\gamma} \rho_{\gamma} \Bigg[& \int_0^1 d\lambda_1 \int d\mathbf{r} \frac{\partial u_{\alpha\gamma}(|\mathbf{r} - \mathbf{r}_{\alpha}|;\lambda_1,\lambda_2 = 0)}{\partial\lambda_1} \\ & \times g_{\gamma}(;\lambda_1,\lambda_2 = 0) \\ & + \int_0^1 d\lambda_2 \int d\mathbf{r} \frac{\partial u_{\alpha\gamma}(|\mathbf{r} - \mathbf{r}_{\alpha}|;\lambda_1 = 1,\lambda_2)}{\partial\lambda_2} \\ & \times g_{\gamma}(\mathbf{r};\lambda_1 = 1,\lambda_2) \Bigg]\end{aligned} \tag{14}$$

After calculating $\Delta\mu_\alpha$ once, it becomes possible to reproduce the contributions of amino acid residues or main/side chains. A similar expression was derived for the solvation entropy,[71] but we used the temperature derivative of the SFE at constant solvent density:

$$\Delta S_i = -\left(\frac{\partial\Delta\mu_i}{\partial T}\right)_{\rho} \tag{15}$$

To calculate $\Delta\mu_\alpha$, we need $h_\gamma(\mathbf{r};\lambda_1,\lambda_2)$, which is obtained using the 3D-RISM theory. For a solute−solvent system at infinite dilution, the 3D-RISM equation can be written as follows:

$$h_{\gamma}(\mathbf{r};\lambda_1,\lambda_2) = \sum_{\gamma'} c_{\gamma'}(\mathbf{r};\lambda_1,\lambda_2) * [w_{\gamma'\gamma}^{vv}(r) + \rho_{\gamma'} h_{\gamma'\gamma}^{vv}(r)] \tag{16}$$

where $h_\gamma(\mathbf{r};\lambda_1,\lambda_2)$ and $c_\gamma(\mathbf{r};\lambda_1,\lambda_2)$ are, respectively, the 3D total and direct correlation functions of the solvent site, γ, around the solute under λ_1 and λ_2, where the asterisk $(*)$ denotes a convolution integral in real space, $w_{\gamma'\gamma}^{vv}(r)$ is the site−site intramolecular correlation function of the solvent, and $h_{\gamma'\gamma}^{vv}(r)$ is the site−site total correlation function of the pure solvent. $h_{\gamma'\gamma}^{vv}(r)$ was precalculated using the 1D-RISM theory for a pure solvent. The 3D-RISM equation was complemented by the Kovalenko−Hirata (KH) closure equation, as follows:

$$\begin{aligned} h_{\gamma}(\mathbf{r};\lambda_1,\lambda_2) &= \begin{cases} \exp(\chi_{\gamma}) - 1 & (\chi_{\gamma} < 0) \\ \chi_{\gamma} & (\chi_{\gamma} \geq 0) \end{cases} \\ \chi_{\gamma} &= -\beta u_r(\mathbf{r};\lambda_1,\lambda_2) + h_{\gamma}(\mathbf{r};\lambda_1,\lambda_2) - c_{\gamma}(r;\lambda_1,\lambda_2) \end{aligned} \tag{17}$$

where $\beta = 1/(k_B T)$ is the reciprocal of the thermodynamic temperature, where k_B is the Boltzmann constant and T is the temperature. Finally, the 3D distribution function, $g_\gamma(\mathbf{r};\lambda_1,\lambda_2)$, is defined from $h_\gamma(\mathbf{r};\lambda_1,\lambda_2)$ as follows:

$$g_{\gamma}(\mathbf{r};\lambda_1,\lambda_2) = h_{\gamma}(\mathbf{r};\lambda_1,\lambda_2) + 1 \tag{18}$$

We calculated $g_\gamma(\mathbf{r};\lambda_1,\lambda_2)$ at every integration step of eq 14.

The atomic decomposition method is a powerful method that can calculate the contribution of every single atom in a protein; however, it is computationally expensive. In the present study, a total of 63 calculations were performed for the integration of λ_1 and λ_2 in eq 14. Thus, we used the reference-modified density functional theory (RMDFT) functional,[77−79] which requires only one 3D-RISM calculation to calculate the SFE of the whole protein. We introduced a hard-sphere (HS) reference system to the DFT for polyatomic molecular liquids

https://doi.org/10.1021/acsomega.3c05809
ACS Omega 2023, 8, 43827−43835

from which we derived the functional of a solute molecule in water. The RMDFT functional is expressed as follows:

$$\begin{aligned}\Delta\mu_{\mathrm{RMDFT}} = &-\frac{1}{\beta}\sum_{\gamma}\rho_{\gamma}\int \mathrm{d}\mathbf{r} h_{\gamma}(\mathbf{r}) \\ &+ \frac{\rho}{\beta}\sum_{\gamma}\sum_{\gamma'}\rho_{\gamma}\int \mathrm{d}\mathbf{r}\int \mathrm{d}\mathbf{r}' C^{ex}_{\gamma\gamma'}(|\mathbf{r}-\mathbf{r}'|)h_{\gamma}(\mathbf{r}) \\ &+ \frac{1}{2\beta}\sum_{\gamma}\sum_{\gamma'}\rho_{\gamma}\rho'_{\gamma}\int \mathrm{d}\mathbf{r}\int \mathrm{d}\mathbf{r}' C^{ex}_{\gamma\gamma'}(|\mathbf{r}-\mathbf{r}'|) \\ &\times h_{\gamma}(\mathbf{r})h_{\gamma'}(\mathbf{r}') \\ &+ \Delta F^{\mathrm{HS}}[\rho_{\mathrm{O}}] - \rho_{\mathrm{O}}\int \mathrm{d}\mathbf{r}\left[\frac{\delta F^{\mathrm{HS}}[\rho_{\mathrm{O}}]}{\delta(\rho_{\mathrm{O}}h_{\mathrm{O}}(\mathbf{r}))}(h_{\mathrm{O}}(\mathbf{r})+1) \right. \\ &\left. - \mu_{\mathrm{O}}^{\mathrm{HS}}\right] \end{aligned} \tag{19}$$

where

$$C^{ex}_{\alpha\beta}(r) = \begin{cases} \bar{C}_{\mathrm{OO}}(r) - C^{\mathrm{HS}}_{\mathrm{OO}}(r) & (\alpha=\beta=\mathrm{O}) \\ \bar{C}_{\alpha\beta}(r) & (\text{otherwise}) \end{cases}$$

$$\bar{C}_{\alpha\beta}(r) = C_{\alpha\beta}(r) + C^{\mathrm{IM}}_{\alpha\beta}(r)$$

$$\tilde{C}_{\alpha\beta}(k) = \frac{\delta_{\alpha\beta}}{\rho} - \left[\delta_{\alpha\beta}\rho + (1-\delta_{\alpha\beta})\rho\frac{\sin(kL_{\alpha\beta})}{kL_{\alpha\beta}}\right]^{-1} \tag{20}$$

Here, $C_{\alpha\beta}(r)$ is the site−site direct correlation function of the pure solvent, $C^{\mathrm{IM}}_{\alpha\beta}(r)$ is the intramolecular direct correlation function,[80] $L_{\alpha\beta}$ is the length of the bond between the α and β sites, O denotes the oxygen site of the water solvent, $C^{\mathrm{HS}}_{\mathrm{OO}}(r)$ corresponds to the site−site direct correlation function of the reference HS fluid, $F^{\mathrm{HS}}[\rho_{\mathrm{O}}]$ is the excess intrinsic free energy functional for the HS fluid, $\mu^{\mathrm{HS}}_{\mathrm{OO}}$ is the excess chemical potential of the reference HS fluid, $\delta_{\alpha\beta}$ is the Kronecker delta, and ρ is the number density of the water solvent. Therefore, we require the theory for HS fluids, e.g., the effective density approximation (EDA) theory.[81] Using this functional, the SFE can be obtained simply by performing a 3D-RISM calculation under λ_1=λ_2 = 1.

COMPUTATIONAL DETAILS

In this study, we used the K8A mutant of the thermostable Trp-cage variant TC10b.[65] Details of the MD simulation of the Trp-cage on the Anton supercomputer can be found in the Supporting Information of ref. 82. As the CHARMM22* force field[83,84] was used for the MD simulation, we used the same force field in this study. Structures were extracted from the MD trajectory for our calculations and used in intervals of 20 ns, which correspond to every 100 samples. The total number of sampled structures was 10 440. We used GROMACS[85] for calculating the conformational energy. The SFE of the proteins was calculated using the 3D-RISM theory[74,75] with the RMDFT functional[77−79] and with the atomic decomposition method.[70,72,73] We used the TIP3P water model with additional parameters (σ = 0.4 Å and ϵ = 0.046 kcal mol^{-1}).[86,87] The number density of water was 0.033329 $^{-3}$ for the thermodynamic states at room temperature (298.15K). We employed the EDA theory to calculate $C^{\mathrm{HS}}_{\mathrm{OO}}(r)$. The optimal HS diameter for the water oxygen was 2.88 for the RMDFT functional. We chose this diameter so that the solvation free energies of methane, butane, and isopropane match the experimental values in the aqueous solvent (the TIP3 model with additional parameters).[77,78] The 3D-RISM/KH equations were solved on a grid of 256^3 points in a cubic cell of 128^3 Å^3. The atomic decomposition calculations were performed using 0.05 as the increment width of λ_1 and used the following numbers as λ_2 ticks: 0.001, 0.005, 0.01, and then from 0.025 to 1.0 in increments of 0.025. The temperature derivative for the solvation entropy calculation was obtained during the first-order difference with ΔT = 2 K. We performed the SFE calculation using the 3D-RISM theory with the original code for multi-GPU processing.[88−90]

RESULTS AND DISCUSSION

First, we describe the computation of the native and unfolded states. The values of the total energy (upper) and the end-to-end distance between the C_α atoms of the N- and C-termini (lower) of the Trp-cage are shown in Figure 2 as a function of C_α-RMSD with respect to the structure with the lowest total energy. The most stable structure has a total energy of −205.5 kcal/mol, and the C_α-RMSD value is 0 Å. Assuming an allowable energy fluctuation of 0.5 kcal/mol per residue, and the fact that the Trp-cage is a 20-residue protein, the overall

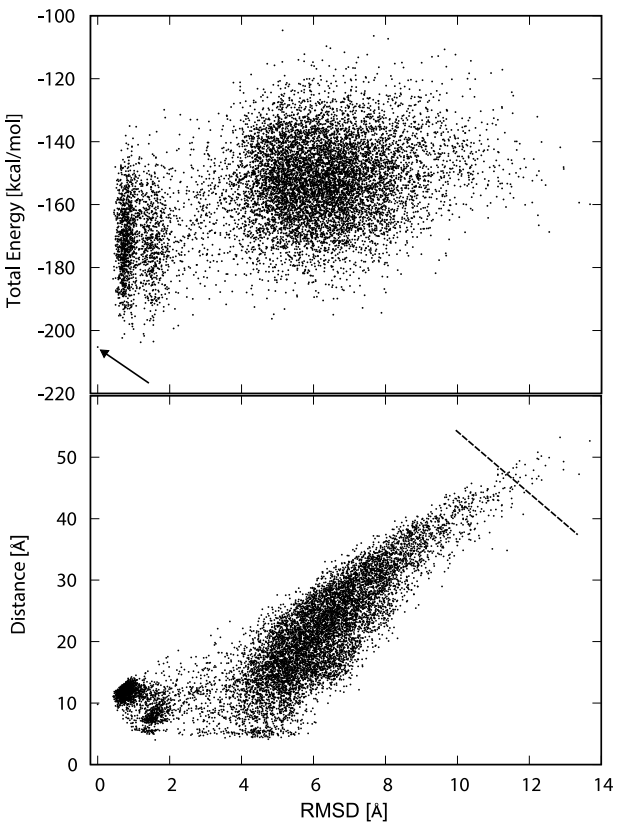

Figure 2. Upper panel: Total energy as a function of C_α-RMSD with respect to the most stable structure in the simulation. The arrow indicates the most stable structure. Lower panel: End-to-end distance as a function of the C_α-RMSD with respect to the most stable structure in the simulation. The structure above (and to the right) the dashed line was defined as the unfolded state.

https://doi.org/10.1021/acsomega.3c05809
ACS Omega 2023, 8, 43827−43835

energy value was estimated to be 10 kcal/mol. We then defined a native state as 29 strctures within 10.0 kcal/mol of the total energy value (i.e, −205.5 kcal/mol). Even if this threshold was changed, it would not result in a qualitative difference in the following discussion. The C_α-RMSD values of these structures were separated and clustered around 1.0 and 1.6 Å. This separation is discussed later. In contrast, the unfolded state was selected as 29 structures with large C_α-RMSD values and end-to-end distances. The structures on the upper right side of the dashed line in the bottom panel of Figure 2 correspond to the unfolded state.

Figure 3 shows the backbone structures of the Trp-cage with the side chains of Asp1, Asp9, and Arg16. Figure 3a shows the

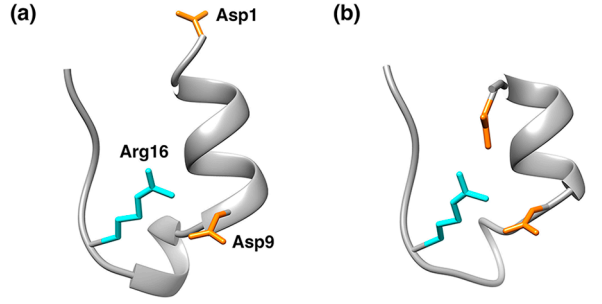

Figure 3. Backbone structures with selected side chains: (a) most stable structure and (b) structure with the lowest total energy near the C_α-RMSD value of 1.6 Å. The orange residues are Asp1 and Asp6, and the cyan residue is Arg16.

most stable structure, and Figure 3b shows the structure with the lowest total energy near the C_α-RMSD value of 1.6 in Figure 2. Although the structure in Figure 3b is similar to the most stable structure in Figure 3a, the N-terminus is closer to the C-terminus. The side chain of Asp1 forms a hydrogen bond with the side chain of Arg16. Hereafter, these two structures are referred to as the native1 and native2 structures, respectively. The side chain of Arg16 forms a hydrogen bond with the side chain of Asp9 in the stable structure of the Trp-cage.[27,29,37,63,65,68,91,92] In Figure 3b, the side chain of Arg16 forms hydrogen bonds with the side chains of both Asp1 and Asp9. The Trp-cage repeatedly forms and breaks hydrogen bonds between Asp1 and Arg16, moving back and forth between these two structures. The period of this oscillation was ∼60 ns, whereas the hydrophobic core of these structures was retained for a few μs in the MD simulation at 290 K.[55] The structural change occurring between these two structures was rapid, making it difficult to distinguish between them. In subsequent calculations, these two structures were processed in their native state.

We then calculated the value of the solvation entropy term, $-T\Delta S$, as a function of the C_α-RMSD, as shown in Figure 4. The difference in the solvation entropy, ΔS is known to be attributable to the effect of the excluded volume. The structures in the region with C_α-RMSD values above 10 have a higher value of the solvation entropy term, $-T\Delta S$, because the Trp-cage has extended structures, which have a larger excluded volume for water. In the region with C_α-RMSD values between 4 and 8, the solvation entropy term forms a large domain with a range of values approximating 25 kcal/mol. This is due to the presence of various metastable structures that are more compact than the extended structures. The solvation entropy term clearly has a lower value in regions

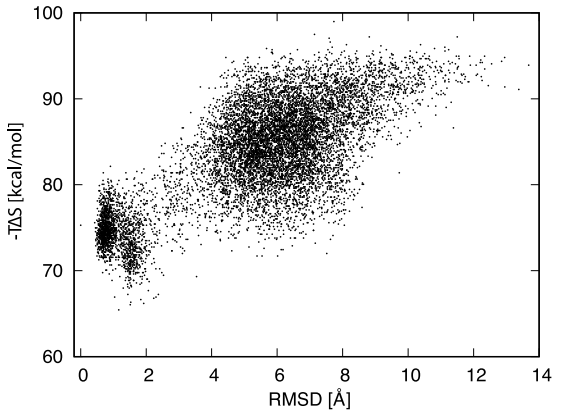

Figure 4. Solvation entropy term as a function of the C_α-RMSD with respect to the most stable structure in the simulation.

with C_α-RMSD values below 2 Å. The more compact the structure of the Trp-cage, the lower the solvation entropy term, that is, the smaller the excluded volume of water. During the conformational change from native1 to native2, the side chains of Asp1 and Arg16 were dehydrated and formed hydrogen bonds. The solvation entropy, S, increases when the Asp1 side chain forms a hydrogen bond with the Arg16 side chain. The formation of hydrogen bonds by these hydrophilic side chains results in an energy gain from the solvation entropy due to dehydration. The average total energy difference from the native state to the unfolded state was 62.4 kcal/mol, where the positive value indicates that the native state was stable. The difference in the average solvation entropy term was 31.3 kcal/mol, which is half the difference in the average total energy. The solvation entropy contributes significantly to the Trp-cage folding. A comparison of the native1 and native 2 regions reveals that the native2 region has lower values of the solvation entropy term, whereas the native1 region has lower total energy values. The results indicate that for the structures with similar excluded volumes, we need to incorporate other energy terms to investigate the stabilization in details.[5]

The total energy stability of each residue and its main and side chains are shown in Figure 5. The extent to which the main chain or side chain contributes depends on the residue. All of the residues, with the exception of Gly11, stabilized the native structure. Gly11 forms a short 3_{10}-helix with Pro12 and

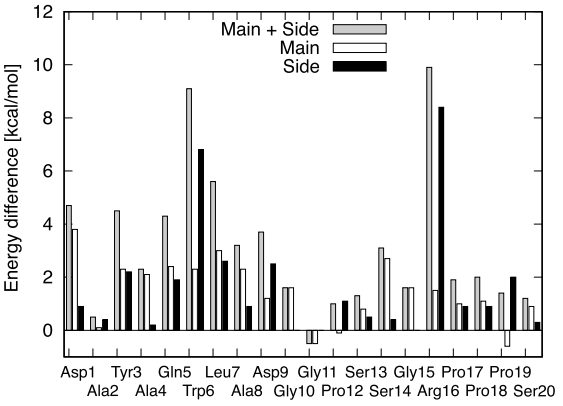

Figure 5. Differences in the average total energy of each residue of the unfolded state from that in the native state. Gray, white, and black indicate the sum of the main and side chains, main chain, and side chain, respectively.

https://doi.org/10.1021/acsomega.3c05809
ACS Omega 2023, 8, 43827−43835

Ser13, and the total energy difference between these helices is positive. However, the 3_{10}-helix makes only a small contribution to the structural stability of the Trp-cage, whereas the α-helix, consisting of Ala2−Ala8, contributes significantly. In particular, the contribution of the side chain of Trp6 to the structural stability is 6.8 kcal/mol. The contribution of the hydrophobic core formed by Tyr3, Leu7, Pro12, Pro18, and Pro19 around Trp6 was 15.6 kcal/mol. The side chain of Trp6 also formed a hydrogen bond with the main chain of Arg16, and the contribution of the main chain of Arg16 was 1.5 kcal/mol. The largest contribution to the overall stability of the Trp-cage, 8.4 kcal/mol, was observed for the side chain of Arg16. The contribution of the side chain of Asp9, which forms a salt bridge with Arg16, was 2.5 kcal/mol. The contribution of the salt bridge was 10.9 kcal/mol, the second only to that of the hydrophobic core.

The total energy, conformational energy, and SFE differences in the (a) main and (b) side chains are shown in Figure 6. Both the main and side chains gain conformational energy at

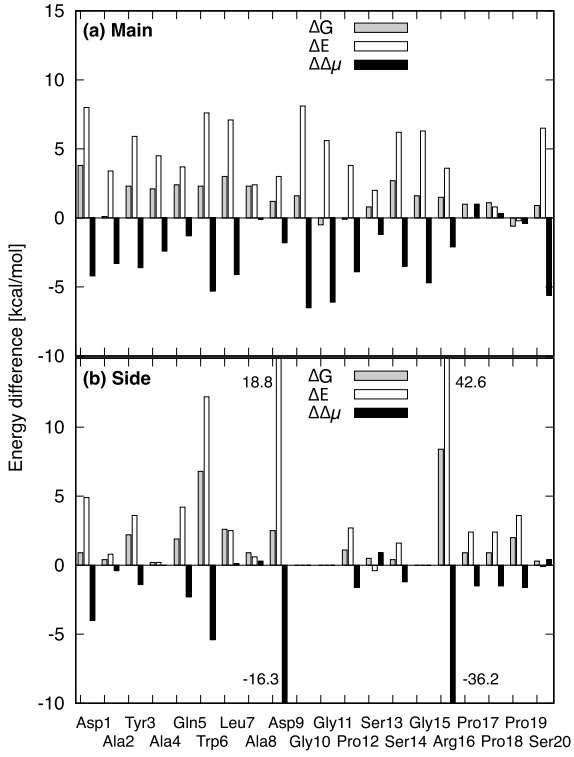

Figure 6. Differences in the average total energy (gray), average conformational energy (white), and average SFE (black) in (a) main and (b) side chains of each residue of the unfolded state from that of the native state.

the cost of the SFE during the folding process. This indicated that both the main and side chains were dehydrated to form hydrogen bonds within the protein. However, to increase their energy, the side chains competed more aggressively than the main chains, because the main chains were less exposed to the surrounding solvent than the side chains. Gly, which does not have a side chain, competed in a slightly larger range of energy than the other amino acids. The magnitude of the competition for energy by the side chains varies depending on whether the side chain is hydrophilic or hydrophobic. Hydrophilic side chains gain a greater amount of conformational energy and lose a larger amount of SFE. Therefore, the total energy difference of the hydrophilic side chain was not significantly different from that of the hydrophobic side chains. The hydrophilic side chains, Asp9 and Arg16, lose more SFE because of dehydration but also gain more conformational energy by forming hydrogen bonds within the protein. The hydrophobic residue Trp6 exhibited a smaller conformational energy gain and SFE loss than Asp9 and Arg16. However, the total energy gain was larger for Arg16, Trp6, and Asp9, in that order, depending on the amino acid sequence and native structure.

Figure 7 shows the differences in the average solvation entropy term for each amino acid. The contributions of the

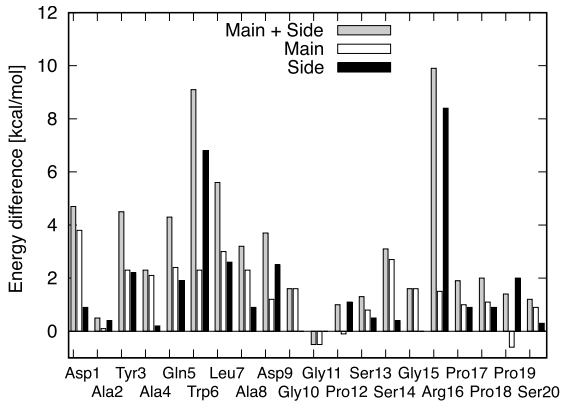

Figure 7. Differences in the average solvation entropy of each residue of the unfolded state from those of the native state. Gray, white, and black indicate the sum of the main and side chains, main chain, and side chain, respectively.

solvation entropy term of the main and side chains in the entire Trp-cage are 17.4 and 13.9 kcal/mol, respectively. The contribution of the main chain to the solvation entropy is 3.5 kcal/mol larger than that of the side chains. In particular, Gly10 and Gly11, which do not have side chains, have relatively high values of 1.8 and 2.1 kcal/mol, respectively. The contribution of Gly11 was slightly higher because it is buried inside the protein, possibly due to the absence of side chains, which contribute to the compact structure of the Trp-cage. The sum of contributions of these two residues is 3.9 kcal/mol, which is almost equal to the difference between the contributions of the main and side chains. In other words, excluding the contribution of the main chains of the Gly residues, the solvation entropy contributions of the main and side chains are almost equal.

The contributions of secondary structures, hydrophobic core, and salt bridge were also taken into account. The contribution of the 3_{10}-helix from Gly11 to Ser14 is 4.5 kcal/mol and that of the α-helix is 14.3 kcal/mol. Notably, the latter contribution includes those of the side chains of Tyr3, Trp6, and Leu7 (5.1 kcal/mol in total), which form the hydrophobic core. The formations of secondary structures such as α-helix and 3_{10}-helix contributed significantly to the increase in the solvation entropy term. The contribution of the hydrophobic core is 6.3 kcal/mol, which corresponds to 20% of the total solvation entropy term. However, the contributions of Pro12, Pro18, and Pro19, amounting to 0.4, 0.0, and 0.8 kcal/mol, respectively, were not significant. As Barua et al. pointed out, Pro/Trp interactions are not essential for the formation of a hydrophobic core.[65] Hałabis et al. conducted NMR experiments to show that the Trp6-Arg16 interaction remains, but

https://doi.org/10.1021/acsomega.3c05809
ACS Omega 2023, 8, 43827−43835

the Trp6-Pro12 interaction disappears at 313 K.[58] The formation of the salt bridge between the Asp9 and Arg16 side chains increases the solvation entropy term by 5.0 kcal/mol. Although these hydrophilic side chains are exposed to the solvent, the formation of salt bridges increases the solvation entropy. This indicates that the solvation entropy, which is the source of hydrophobic interactions, plays a major role in Trp-cage protein folding.

CONCLUSION

Using the atomic decomposition method, we investigated the contribution of the main and side chains of individual amino acids to folding of the Trp-cage. In particular, we focused on the hydrophobic core centered on the side chain of Trp6 and the salt bridge formed by the side chains of Asp9 and Arg16. The contributions of the hydrophobic core to the total energy and solvation entropy were 15.6 and 6.3 kcal/mol, respectively, and the corresponding contributions by the salt bridge were 10.9 and 5.0 kcal/mol, respectively. The sum of these total energy contributions corresponds to 42% of the total energy gain of the Trp-cage. More specifically, the gain attributable to the solvation entropy was equivalent to 36%. Particularly interesting is that not only the hydrophobic core but also the salt bridge formation of the hydrophilic side chains contributes to the energy gain of the Trp-cage due to the solvation entropy. This insight highlights the pivotal role of solvation entropy and the indirect influence of aqueous solvents on the structural stability of a protein.

The analysis of the energy gain of the main and side chains of the amino acids of proteins using the atomic decomposition method deepens our understanding of the principles of protein stability and folding dynamics. This methodology emerges as a potent tool in investigations related to protein stabilization, destabilization, and conformational ramifications brought about by amino acid mutations. Such detailed analyses are indispensable for the rational design of proteins, enabling enhanced functionalities and, more broadly, a deeper comprehension of protein mutations and their effects on stability. The implications of our study extend beyond mere understanding, potentially paving the way for pioneering endeavors in de novo protein design, conceiving folding architectures previously uncharted in natural systems.

AUTHOR INFORMATION

Corresponding Author

Yutaka Maruyama − *Data Science Center for Creative Design and Manufacturing, The Institute of Statistical Mathematics, Tachikawa, Tokyo 190-8562, Japan; Department of Physics, School of Science and Technology, Meiji University, Kawasaki-shi, Kanagawa 214-8571, Japan;* orcid.org/0000-0003-4035-4885; Email: drmaru@ism.ac.jp

Author

Ayori Mitsutake − *Department of Physics, School of Science and Technology, Meiji University, Kawasaki-shi, Kanagawa 214-8571, Japan;* orcid.org/0000-0002-4194-7255

Complete contact information is available at: https://pubs.acs.org/10.1021/acsomega.3c05809

Notes

The authors declare no competing financial interest.

ACKNOWLEDGMENTS

This study was supported by JSPS KAKENHI, grant no. JP20H03230 and JP22H04756. The numerical calculations were conducted in part using Cygnus and Pegasus at the Center for Computational Sciences, University of Tsukuba. Molecular graphics were designed using UCSF Chimera, developed by the Resource for Biocomputing, Visualization, and Informatics at the University of California, San Francisco.[93]

REFERENCES

(1) Jumper, J.; Evans, R.; Pritzel, A.; Green, T.; Figurnov, M.; Ronneberger, O.; Tunyasuvunakool, K.; Bates, R.; Žídek, A.; Potapenko, A.; et al. Highly accurate protein structure prediction with AlphaFold. *Nature* **2021**, *596*, 583−589.

(2) Baek, M.; DiMaio, F.; Anishchenko, I.; Dauparas, J.; Ovchinnikov, S.; Lee, G. R.; Wang, J.; Cong, Q.; Kinch, L. N.; Schaeffer, R. D.; et al. Accurate prediction of protein structures and interactions using a three-track neural network. *Science* **2021**, *373*, 871−876.

(3) Maruyama, Y.; Harano, Y. Does water drive protein folding? *Chem. Phys. Lett.* **2013**, *581*, 85−90.

(4) Maruyama, Y.; Mitsutake, A. Stability of unfolded and folded protein structures using a 3D-RISM with the RMDFT. *J. Phys. Chem. B* **2017**, *121*, 9881−9885.

(5) Maruyama, Y.; Mitsutake, A. Analysis of Structural Stability of Chignolin. *J. Phys. Chem. B* **2018**, *122*, 3801−3814.

(6) Maruyama, Y.; Koroku, S.; Imai, M.; Takeuchi, K.; Mitsutake, A. Mutation-induced change in chignolin stability from π-turn to α-turn. *RSC Adv.* **2020**, *10*, 22797−22808.

(7) Maruyama, Y.; Mitsutake, A. Structural Stability Analysis of Proteins Using End-to-End Distance: A 3D-RISM Approach. *J* **2022**, *5*, 114−125.

(8) Neidigh, J. W.; Fesinmeyer, R. M.; Andersen, N. H. Designing a 20-residue protein. *Nat. Struct. Biol.* **2002**, *9*, 425−430.

(9) Gellman, S. H.; Woolfson, D. N. Mini-proteins Trp the light fantastic. *Nat. Struct. Biol.* **2002**, *9*, 408−410.

(10) Qiu, L.; Pabit, S. A.; Roitberg, A. E.; Hagen, S. J. Smaller and Faster: The 20-Residue Trp-Cage Protein Folds in 4 μs. *J. Am. Chem. Soc.* **2002**, *124*, 12952−12953.

(11) Iavarone, A. T.; Parks, J. H. Conformational Change in Unsolvated Trp-cage Protein Probed by Fluorescence. *J. Am. Chem. Soc.* **2005**, *127*, 8606−8607.

(12) Hudáky, P.; Stráner, P.; Farkas, V.; Váradi, G.; Tóth, G.; Perczel, A. Cooperation between a Salt Bridge and the Hydrophobic Core Triggers Fold Stabilization in a Trp-Cage Miniprotein. *Biochemistry* **2008**, *47*, 1007−1016.

(13) Marinelli, F. Following Easy Slope Paths on a Free Energy Landscape: The Case Study of the Trp-Cage Folding Mechanism. *Biophys. J.* **2013**, *105*, 1236−1247.

(14) Meuzelaar, H.; Marino, K. A.; Huerta-Viga, A.; Panman, M. R.; Smeenk, L. E. J.; Kettelarij, A. J.; van Maarseveen, J. H.; Timmerman, P.; Bolhuis, P. G.; Woutersen, S. Folding Dynamics of the Trp-Cage Miniprotein: Evidence for a Native-Like Intermediate from Combined Time-Resolved Vibrational Spectroscopy and Molecular Dynamics Simulations. *J. Phys. Chem. B* **2013**, *117*, 11490−11501.

(15) Han, W.; Schulten, K. Characterization of Folding Mechanisms of Trp-Cage and WW-Domain by Network Analysis of Simulations with a Hybrid-Resolution Model. *J. Phys. Chem. B* **2013**, *117*, 13367−13377.

(16) Miao, Y.; Feixas, F.; Eun, C.; McCammon, J. A. Accelerated molecular dynamics simulations of protein folding. *J. Comput. Chem.* **2015**, *36*, 1536−1549.

(17) Zhou, C.-Y.; Jiang, F.; Wu, Y.-D. Folding Thermodynamics and Mechanism of Five Trp-Cage Variants from Replica-Exchange MD Simulations with RSFF2 Force Field. *J. Chem. Theory Comput.* **2015**, *11*, 5473−5480.

(18) Andryushchenko, V. A.; Chekmarev, S. F. A hydrodynamic view of the first-passage folding of Trp-cage miniprotein. *Eur. Biophys. J.* **2016**, *45*, 229−243.
(19) Borgohain, G.; Paul, S. Atomistic level understanding of the stabilization of protein Trp cage in denaturing and mixed osmolyte solutions. *Comput. Theor. Chem.* **2018**, *1131*, 78−89.
(20) Chalyavi, F.; Schmitz, A. J.; Tucker, M. J. Unperturbed Detection of the Dynamic Structure in the Hydrophobic Core of Trp-Cage via Two-Dimensional Infrared Spectroscopy. *J. Phys. Chem. Lett.* **2020**, *11*, 832−837.
(21) Yasuda, T.; Shigeta, Y.; Harada, R. The Folding of Trp-cage is Regulated by Stochastic Flip of the Side Chain of Tryptophan. *Chem. Lett.* **2021**, *50*, 162−165.
(22) Coe, M. K.; Evans, R.; Wilding, N. B. Understanding the physics of hydrophobic solvation. *J. Chem. Phys.* **2023**, *158*, 034508.
(23) Bunagan, M. R.; Yang, X.; Saven, J. G.; Gai, F. Ultrafast Folding of a Computationally Designed Trp-Cage Mutant: Trp ^{2} -Cage. *J. Phys. Chem. B* **2006**, *110*, 3759−3763.
(24) Ahmed, Z.; Beta, I. A.; Mikhonin, A. V.; Asher, S. A. UV-Resonance Raman Thermal Unfolding Study of Trp-Cage Shows That It Is Not a Simple Two-State Miniprotein. *J. Am. Chem. Soc.* **2005**, *127*, 10943−10950.
(25) Lin, M.; Ahmed, Z.; Taormina, C. R.; Somayajula, K. V. A quadrupole/time-of-flight mass spectrometry study of trp-cage's conformation. *J. Am. Soc. Mass Spectrom.* **2007**, *18*, 195−200.
(26) Pitera, J. W.; Swope, W. Understanding folding and design: Replica-exchange simulations of "Trp-cage" miniproteins. *Proc. Natl. Acad. Sci. U.S.A.* **2003**, *100*, 7587−7592.
(27) Zhou, R. Trp-cage: Folding free energy landscape in explicit water. *Proc. Natl. Acad. Sci. U.S.A.* **2003**, *100*, 13280−13285.
(28) Ota, M.; Ikeguchi, M.; Kidera, A. Phylogeny of protein-folding trajectories reveals a unique pathway to native structure. *Proc. Natl. Acad. Sci. U.S.A.* **2004**, *101*, 17658−17663.
(29) Ding, F.; Buldyrev, S. V.; Dokholyan, N. V. Folding Trp-Cage to NMR Resolution Native Structure Using a Coarse-Grained Protein Model. *Biophys. J.* **2005**, *88*, 147−155.
(30) Juraszek, J.; Bolhuis, P. G. Sampling the multiple folding mechanisms of Trp-cage in explicit solvent. *Proc. Natl. Acad. Sci. U.S.A.* **2006**, *103*, 15859−15864.
(31) Paschek, D.; Nymeyer, H.; García, A. E. Replica exchange simulation of reversible folding/unfolding of the Trp-cage miniprotein in explicit solvent: On the structure and possible role of internal water. *J. Struct. Biol.* **2007**, *157*, 524−533.
(32) Juraszek, J.; Bolhuis, P. G. Rate Constant and Reaction Coordinate of Trp-Cage Folding in Explicit Water. *Biophys. J.* **2008**, *95*, 4246−4257.
(33) Kannan, S.; Zacharias, M. Folding of Trp-cage Mini Protein Using Temperature and Biasing Potential Replica—Exchange Molecular Dynamics Simulations. *Int. J. Mol. Sci.* **2009**, *10*, 1121−1137.
(34) Lai, Z.; Preketes, N. K.; Mukamel, S.; Wang, J. Monitoring the Folding of Trp-Cage Peptide by Two-Dimensional Infrared (2DIR) Spectroscopy. *J. Phys. Chem. B* **2013**, *117*, 4661−4669.
(35) Dickson, A., III; Brooks, C. L., III Native States of Fast-Folding Proteins Are Kinetic Traps. *J. Am. Chem. Soc.* **2013**, *135*, 4729−4734.
(36) Ota, M.; Ikeguchi, M.; Kidera, A. Itinerary profiling to analyze a large number of protein-folding trajectories. *Biophys. Physicobiol.* **2016**, *13*, 295−304.
(37) Iavarone, A. T.; Patriksson, A.; van der Spoel, D.; Parks, J. H. Fluorescence Probe of Trp-Cage Protein Conformation in Solution and in Gas Phase. *J. Am. Chem. Soc.* **2007**, *129*, 6726−6735.
(38) Ren, H.; Lai, Z.; Biggs, J. D.; Wang, J.; Mukamel, S. Two-dimensional stimulated resonance Raman spectroscopy study of the Trp-cage peptide folding. *Phys. Chem. Chem. Phys.* **2013**, *15*, 19457−19464.
(39) Piana, S.; Laio, A. A Bias-Exchange Approach to Protein Folding. *J. Phys. Chem. B* **2007**, *111*, 4553−4559.
(40) Marinelli, F.; Pietrucci, F.; Laio, A.; Piana, S. A Kinetic Model of Trp-Cage Folding from Multiple Biased Molecular Dynamics Simulations. *PLoS Comput. Biol.* **2009**, *5*, No. e1000452.
(41) Zheng, W.; Gallicchio, E.; Deng, N.; Andrec, M.; Levy, R. M. Kinetic Network Study of the Diversity and Temperature Dependence of Trp-Cage Folding Pathways: Combining Transition Path Theory with Stochastic Simulations. *J. Phys. Chem. B* **2011**, *115*, 1512−1523.
(42) Shao, Q.; Shi, J.; Zhu, W. Enhanced sampling molecular dynamics simulation captures experimentally suggested intermediate and unfolded states in the folding pathway of Trp-cage miniprotein. *J. Chem. Phys.* **2012**, *137*, 125103.
(43) Kim, S. B.; Dsilva, C. J.; Kevrekidis, I. G.; Debenedetti, P. G. Systematic characterization of protein folding pathways using diffusion maps: Application to Trp-cage miniprotein. *J. Chem. Phys.* **2015**, *142*, 085101.
(44) Omelyan, I.; Kovalenko, A. MTS-MD of Biomolecules Steered with 3D-RISM-KH Mean Solvation Forces Accelerated with Generalized Solvation Force Extrapolation. *J. Chem. Theory Comput.* **2015**, *11*, 1875−1895.
(45) Zhang, T.; Nguyen, P. H.; Nasica-Labouze, J.; Mu, Y.; Derreumaux, P. Folding Atomistic Proteins in Explicit Solvent Using Simulated Tempering. *J. Phys. Chem. B* **2015**, *119*, 6941−6951.
(46) Kamiya, M.; Sugita, Y. Flexible selection of the solute region in replica exchange with solute tempering: Application to protein-folding simulations. *J. Chem. Phys.* **2018**, *149*, 072304.
(47) Harada, R.; Shigeta, Y. Temperature-Shuffled Structural Dissimilarity Sampling Based on a Root-Mean-Square Deviation. *J. Chem. Inf. Model.* **2018**, *58*, 1397−1405.
(48) Harada, R.; Shigeta, Y. How Does Friction Coefficient Affect the Conformational Sampling Efficiency of Parallel Cascade Selection Molecular Dynamics? *Chem. Lett.* **2018**, *47*, 1119−1122.
(49) Harada, R.; Shigeta, Y. Selection Rules for Outliers in Outlier Flooding Method Regulate Its Conformational Sampling Efficiency. *J. Chem. Inf. Model.* **2019**, *59*, 3919−3926.
(50) Harada, R.; Yoshino, R.; Nishizawa, H.; Shigeta, Y. Temperature−pressure shuffling outlier flooding method enhances the conformational sampling of proteins. *J. Comput. Chem.* **2019**, *40*, 1530−1537.
(51) Omelyan, I.; Kovalenko, A. Enhanced solvation force extrapolation for speeding up molecular dynamics simulations of complex biochemical liquids. *J. Chem. Phys.* **2019**, *151*, 214102.
(52) Shin, K.; Tran, D. P.; Takemura, K.; Kitao, A.; Terayama, K.; Tsuda, K. Enhancing Biomolecular Sampling with Reinforcement Learning: A Tree Search Molecular Dynamics Simulation Method. *ACS Omega* **2019**, *4*, 13853−13862.
(53) Meli, M.; Morra, G.; Colombo, G. Simple Model of Protein Energetics To Identify Ab Initio Folding Transitions from All-Atom MD Simulations of Proteins. *J. Chem. Theory Comput.* **2020**, *16*, 5960−5971.
(54) Strahan, J.; Antoszewski, A.; Lorpaiboon, C.; Vani, B. P.; Weare, J.; Dinner, A. R. Long-Time-Scale Predictions from Short-Trajectory Data: A Benchmark Analysis of the Trp-Cage Miniprotein. *J. Chem. Theory Comput.* **2021**, *17*, 2948−2963.
(55) Maruyama, Y.; Igarashi, R.; Ushiku, Y.; Mitsutake, A. Analysis of Protein Folding Simulation with Moving Root Mean Square Deviation. *J. Chem. Inf. Model.* **2023**, *63*, 1529−1541.
(56) Paschek, D.; Hempel, S.; García, A. E. Computing the stability diagram of the Trp-cage miniprotein. *Proc. Natl. Acad. Sci. U.S.A.* **2008**, *105*, 17754−17759.
(57) Rovó, P.; Farkas, V.; Hegyi, O.; Szolomájer-Csikós, O.; Tóth, G. K.; Perczel, A. Cooperativity network of Trp-cage miniproteins: probing salt-bridges. *J. Pept. Sci.* **2011**, *17*, 610−619.
(58) Hałabis, A.; Żmudzińska, W.; Liwo, A.; Ołdziej, S. Conformational Dynamics of the Trp-Cage Miniprotein at Its Folding Temperature. *J. Phys. Chem. B* **2012**, *116*, 6898−6907.
(59) Du, W.; Bolhuis, P. G. Sampling the equilibrium kinetic network of Trp-cage in explicit solvent. *J. Chem. Phys.* **2014**, *140*, 195102.

https://doi.org/10.1021/acsomega.3c05809
ACS Omega 2023, 8, 43827−43835

(60) Lee, I.-H.; Kim, S.-Y. Dynamic Folding Pathway Models of the Trp-Cage Protein. *BioMed. Res. Int.* **2013**, *2013*, 1−9.
(61) Hu, Z.; Tang, Y.; Wang, H.; Zhang, X.; Lei, M. Dynamics and cooperativity of Trp-cage folding. *Arch. Biochem. Biophys.* **2008**, *475*, 140−147.
(62) Chowdhury, S.; Lee, M. C.; Xiong, G.; Duan, Y. Ab initio Folding Simulation of the Trp-cage Mini-protein Approaches NMR Resolution. *J. Mol. Biol.* **2003**, *327*, 711−717.
(63) Kannan, S.; Zacharias, M. Role of Tryptophan Side Chain Dynamics on the Trp-Cage Mini-Protein Folding Studied by Molecular Dynamics Simulations. *PLoS One* **2014**, *9*, No. e88383.
(64) Simmerling, C.; Strockbine, B.; Roitberg, A. E. All-Atom Structure Prediction and Folding Simulations of a Stable Protein. *J. Am. Chem. Soc.* **2002**, *124*, 11258−11259.
(65) Barua, B.; Lin, J. C.; Williams, V. D.; Kummler, P.; Neidigh, J. W.; Andersen, N. H. The Trp-cage: Optimizing the stability of a globular miniprotein. *Protein Eng., Des. Sel.* **2008**, *21*, 171−185.
(66) Jimenez-Cruz, C. A.; Makhatadze, G. I.; Garcia, A. E. Protonation/deprotonation effects on the stability of the Trp-cage miniprotein. *Phys. Chem. Chem. Phys.* **2011**, *13*, 17056−17063.
(67) Wu, X.; Yang, G.; Zu, Y.; Fu, Y.; Zhou, L.; Yuan, X. The Trp-cage miniprotein with single-site mutations: Studies of stability and dynamics using molecular dynamics. *Comput. Theor. Chem.* **2011**, *973*, 1−8.
(68) Byrne, A.; Williams, D. V.; Barua, B.; Hagen, S. J.; Kier, B. L.; Andersen, N. H. Folding Dynamics and Pathways of the Trp-Cage Miniproteins. *Biochemistry* **2014**, *53*, 6011−6021.
(69) Best, R. B.; Zheng, W.; Mittal, J. Balanced Protein−Water Interactions Improve Properties of Disordered Proteins and Non-Specific Protein Association. *J. Chem. Theory Comput.* **2014**, *10*, 5113−5124.
(70) Chong, S.-H.; Ham, S. Atomic decomposition of the protein solvation free energy and its application to amyloid-beta protein in water. *J. Chem. Phys.* **2011**, *135*, 034506.
(71) Chong, S.-H.; Ham, S. Component analysis of the protein hydration entropy. *Chem. Phys. Lett.* **2012**, *535*, 152−156.
(72) Chong, S.-H.; Ham, S. Impact of chemical heterogeneity on protein self-assembly in water. *Proc. Natl. Acad. Sci. U.S.A.* **2012**, *109*, 7636−7641.
(73) Maruyama, Y.; Takano, H.; Mitsutake, A. Analysis of molecular dynamics simulations of 10-residue peptide, chignolin, using statistical mechanics: Relaxation mode analysis and three-dimensional reference interaction site model theory. *Biophys. Physicobiol.* **2019**, *16*, 407−429.
(74) Beglov, D.; Roux, B. An integral equation to describe the solvation of polar molecules in l iquid water. *J. Phys. Chem. B* **1997**, *101*, 7821−7826.
(75) Kovalenko, A.; Hirata, F. Three-dimensional density profiles of water in contact with a solute o f arbitrary shape: A RISM approach. *Chem. Phys. Lett.* **1998**, *290*, 237−244.
(76) Ben-Naim, A.*Molecular Theory of Solutions*; Oxford University Press: New York, 2006.
(77) Sumi, T.; Mitsutake, A.; Maruyama, Y. A solvation-free-energy functional: A reference-modified density functional formulation. *J. Comput. Chem.* **2015**, *36*, 1359−1369.
(78) Sumi, T.; Mitsutake, A.; Maruyama, Y. Erratum: "A solvation-free-energy functional: A reference-modified density functional formulation" [J. Comput. Chem. 2015, 36, 1359−1369]. *J. Comput. Chem.* **2015**, 2009−2011, DOI: 10.1002/jcc.24035.
(79) Maruyama, Y. Correction terms for the solvation free energy functional of three-dimensional reference interaction site model based on the reference-modified density functional theory. *J. Mol. Liq.* **2019**, *291*, 111160.
(80) Chandler, D.; Mccoy, J. D.; Singer, S. J. Density functional theory of nonuniform polyatomic systems. I. General formulation. *J. Chem. Phys.* **1986**, *85*, 5971−5976.
(81) Sumi, T.; Sekino, H. A Self-Consistent Density-Functional Approach for Homogeneous and Inhomogeneous Classical Fluids. *J. Phys. Soc. Jpn.* **2008**, *77*, 034605.
(82) Lindorff-Larsen, K.; Piana, S.; Dror, R. O.; Shaw, D. E. How fast-folding proteins fold. *Science* **2011**, *334*, 517−520.
(83) MacKerell, A. D., Jr.; Bashford, D.; Bellott, M.; Dunbrack, R. L.; Evanseck, J. D.; Field, M. J.; Fischer, S.; Gao, J.; Guo, H.; Ha, S.; et al. All-atom empirical potential for molecular modeling and dynamics studies of proteins. *J. Phys. Chem. B* **1998**, *102*, 3586−3616.
(84) Mackerell, A. D., Jr.; Feig, M.; Brooks, C. L., III Extending the treatment of backbone energetics in protein force fields: Limitations of gas-phase quantum mechanics in reproducing protein conformational distributions in molecular dynamics simulation. *J. Comput. Chem.* **2004**, *25*, 1400−1415.
(85) Pronk, S.; Páll, S.; Schulz, R.; Larsson, P.; Bjelkmar, P.; Apostolov, R.; Shirts, M. R.; Smith, J. C.; Kasson, P. M.; Van Der Spoel, D.; et al. GROMACS 4.5: A high-throughput and highly parallel open source molecular simulation toolkit. *Bioinformatics* **2013**, *29*, 845−854.
(86) Jorgensen, W. L.; Chandrasekhar, J.; Madura, J. D.; Impey, R. W.; Klein, M. L. Comparison of simple potential functions for simulating liquid water. *J. Chem. Phys.* **1983**, *79*, 926−935.
(87) Pettitt, B. M.; Rossky, P. J. Integral-equation predictions of liquid-state structure for waterlike intermolecular potentials. *J. Chem. Phys.* **1982**, *77*, 1451−1457.
(88) Maruyama, Y.; Hirata, F. Modified Anderson method for accelerating 3D-RISM calculations using graphics processing unit. *J. Chem. Theory Comput.* **2012**, *8*, 3015−3021.
(89) Nukada, A.; Maruyama, Y.; Matsuoka, S.High performance 3-D FFT using multiple CUDA GPUs. In *Proceedings of the 5th Annual Workshop on General Purpose Processing with Graphics Processing Units - GPGPU-5*201257−63
(90) Maruyama, Y.; Yoshida, N.; Tadano, H.; Takahashi, D.; Sato, M.; Hirata, F. Massively parallel implementation of 3D-RISM calculation with volumetric 3D-FFT. *J. Comput. Chem.* **2014**, *35*, 1347−1355.
(91) Patriksson, A.; Adams, C. M.; Kjeldsen, F.; Zubarev, R. A.; van der Spoel, D. A Direct Comparison of Protein Structure in the Gas and Solution Phase: The Trp-cage. *J. Phys. Chem. B* **2007**, *111*, 13147−13150.
(92) Scian, M.; Lin, J. C.; Le Trong, I.; Makhatadze, G. I.; Stenkamp, R. E.; Andersen, N. H. Crystal and NMR structures of a Trp-cage mini-protein benchmark for computational fold prediction. *Proc. Natl. Acad. Sci. U.S.A.* **2012**, *109*, 12521−12525.
(93) Pettersen, E. F.; Goddard, T. D.; Huang, C. C.; Couch, G. S.; Greenblatt, D. M.; Meng, E. C.; Ferrin, T. E. UCSF Chimera—A visualization system for exploratory research and analysis. *J. Comput. Chem.* **2004**, *25*, 1605−1612.

https://doi.org/10.1021/acsomega.3c05809
ACS Omega 2023, 8, 43827−43835